Effects of non-quadrupole modes in the detection and parameter estimation of black hole binaries with nonprecessing spins

Vijay Varma

Theoretical Astrophysics 350-17, California Institute of Technology, Pasadena, CA 91125, USA

Parameswaran Ajith

International Centre for Theoretical Sciences, Tata Institute of Fundamental Research, Bangalore 560012, India

We study the effect of non-quadrupolar modes in the detection and parameter estimation of gravitational waves (GWs) from black-hole binaries with nonprecessing spins, using Advanced LIGO. We evaluate the loss of signal-to-noise ratio (SNR) and the systematic errors in the estimated parameters when a quadrupole-mode template family is used to detect GW signals with all the relevant modes. Target signals are constructed by matching numerical-relativity simulations of nonprecessing black hole binaries describing the late inspiral, merger and ringdown with post-Newtonian/effective-one-body waveforms describing the early inspiral. We find that quadrupole-mode templates modeling nonprecessing spins are more effectual in detecting signals with higher modes, as compared to their nonspinning counterparts. This is achieved at the cost of introducing larger systematic biases in estimated parameters. For a given mass ratio, the subdominant modes are more important for aligned (anti-aligned) spins for detection (parameter estimation). Quadrupole-only templates are sufficient (less than 10% loss of detectable volume at a fixed SNR threshold) for the detection of GWs with $q < 4$ for $\chi_{\text{eff}} \sim 0.5$, $q < 6$ for $\chi_{\text{eff}} \sim 0$ and $q < 7$ for $\chi_{\text{eff}} \sim -0.5$. The systematic errors due to neglecting higher modes are larger than the expected $1\,\sigma$ statistical errors at sky and orientation averaged signal-to-noise ratios of 8 for binaries with $(q > 3, M > 200 M_\odot)$ for $\chi_{\text{eff}} \sim 0.5$, $(q > 2, M > 100 M_\odot)$ for $\chi_{\text{eff}} \sim 0$, and $(q > 2, M > 80 M_\odot)$ for $\chi_{\text{eff}} \sim -0.5$. We provide a summary of the regions in the parameter space where neglecting non-quadrupole modes will cause unacceptable loss of detection rates and unacceptably large systematic biases in the estimated parameters.

I. INTRODUCTION AND SUMMARY

We are firmly into the era of gravitational wave (GW) astronomy, with LIGO having made two confident detections of binary black holes [1, 2] and many more expected in upcoming observing runs [3, 4]. Indeed, these first observations have already given us a glimpse of the unique capabilities of GW astronomy. Apart from providing the first direct evidence of the existence of GWs, these observations confirmed the existence of stellar mass black holes that are much more massive than commonly thought by astronomers [5, 6]. They also provided the first evidence of black hole binaries that inspiral under GW emission and merge within the age of the universe. These observations also enabled us to perform the first tests of GR in the highly relativistic and nonlinear regime of gravity – a regime inaccessible by other astronomical observations and laboratory tests [7].

The first LIGO event, termed GW150914, was produced by the merger of two massive black holes. The resultant signal in the detectors contained imprints of the late inspiral and merger of the two holes and the subsequent ringdown of the remnant black hole. The signal was confidently detected by two types of searches. The first one was a search for generic transient signals that are coherent in multiple detectors [8–10]. The signal was detected with higher confidence by matched-filter based searches that use relativistic models of expected signals from coalescing compact binaries [11]. The second signal was produced by the coalescence of two less massive black holes, and the resultant signal in the detector predominantly consisted of the long inspiral. Hence matched-filter based searches were essential for its detection [2].

Matched filtering is the most sensitive search method for extracting signals of known signal shape from noisy data, such as the GW signals from the coalescence (inspiral, merger and ringdown) of binary black holes. The source parameters are then extracted by comparing the data against theoretical templates by means of Bayesian inference [5]. Our ability to optimally detect the signal using matched filtering and to estimate the source parameters using Bayesian inference depends crucially on how faithfully the theoretical templates model the signal present in the data. If the template is a poor representation of the true signal, this can reduce the matched filtering signal-to-noise ratio (SNR), potentially causing non-detection and/or cause unacceptable systematic biases in the estimated parameters. Good waveform templates should be not only *effectual* in the detection (small loss in the SNR), but also *faithful* in parameter estimation (small systematic biases) [12].

Matched-filter based searches for GWs performed to date, including the ones that resulted in detections, have employed templates that model only the leading (quadrupole, or $\ell = 2$, $m = \pm 2$) spherical harmonic modes of the GWs radiated from the binary. The parameter estimation exercise also has largely employed quadrupole mode templates (with the notable exception of one that directly employed numerical relativity (NR) waveforms [14]). This choice is partly dictated by the unavailability of fast-to-evaluate, semi-analytical waveform templates describing the inspiral, merger and ringdown of binary black holes that model the subdominant (non-quadrupole) modes over a sufficiently wide region in the parameter space (e.g., spinning binaries). More importantly, several studies in the past have suggested that the contribution from subdominant modes are appreciable only for very massive binaries with large mass ratios [13, 15–17]. The effect of subdominant modes was thoroughly investigated in the context of the GW150914 event, and the study concluded that the effect of subdominant modes is negligible in the detection and parameter estimation of GW150914 [18, 19].

In a previous study [13], we investigated the effect of subdominant modes in the detection and parameter estimation of a population of nonspinning black hole binaries. We computed the reduction in the the detectable volume and systematic bias in the estimated parameters when quadrupole mode templates are employed in detection and parameter estimation. Here, we extend our previous study to the case of black hole binaries with nonprecessing spins [1].

―――――――

[1] We note that, in a recent paper, Calderon-Bustillo *et al* [20] extended our

<table>
<tr><td colspan="3">q, χ_{1z}, χ_{2z}</td></tr>
</table>

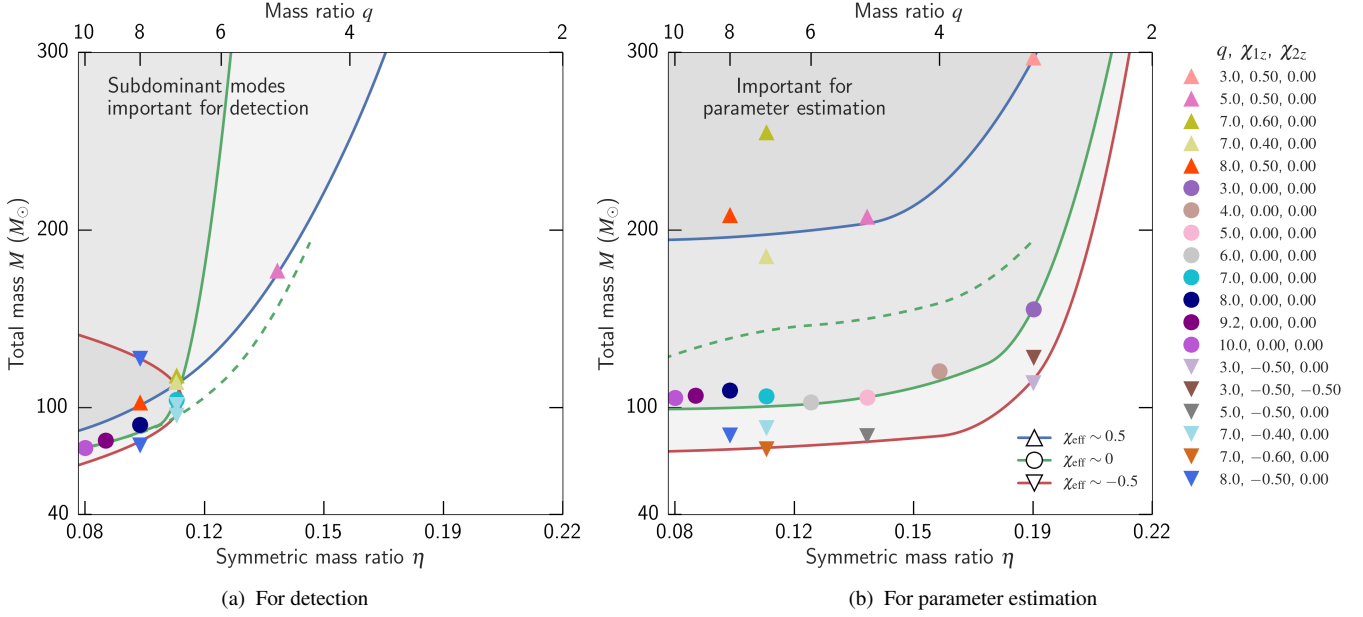(a) For detection   (b) For parameter estimation

FIG. 1: These plots summarize the region in the parameter space of nonprecessing black-hole binaries where contributions from subdominant modes are important for detection (left) and parameter estimation (right). In the left panel, the shaded areas show the regions in the parameter space where the loss of detection volume (for a fixed SNR threshold) due to neglecting subdominant modes is larger than 10%. In the right panel, shaded areas show the regions in the parameter space where the systematic errors in any of the estimated parameters (M, η, $\chi_{\rm eff}$) are larger than the expected statistical errors for a sky and orientation-averaged SNR of 8 (corresponding to an optimal orientation SNR $\simeq 20$). The vertical axes report the total mass M of the binary while horizontal axes report the symmetric mass ratio η (the top horizontal axes show the mass ratio q). In each plot the three solid curves correspond to different effective spin values: blue for $\chi_{\rm eff} \sim 0.5$, green for $\chi_{\rm eff} \sim 0$ and red for $\chi_{\rm eff} \sim -0.5$. The dashed green lines show the same results for nonspinning binaries using a nonspinning template family from our previous work [13], these curves are restricted to $M < 200 M_\odot$. The markers (triangles pointing up/down denoting binaries with aligned/anti-aligned spins and circles denoting nonspinning binaries) indicate the data points that are used to construct the shaded regions and curves. The legend shows the mass ratios and spins of the target signals featured in these plots. See Sec. III for a detailed discussion.

Fig. 1 summarizes the main results from this study. The left plot shows the region in the parameter space where neglecting the subdominant modes will cause an unacceptable (more than 10%) loss in the detectable volume (appropriately averaged over all orientations of the binary) for a fixed SNR threshold. The right plot shows the region in the parameter space where neglecting the subdominant modes will cause unacceptably large systematic bias in the parameter estimation (i.e., systematic errors larger than the expected statistical errors for a sky- and orientation-averaged SNR of 8). Comparing these results with our previous study employing nonspinning templates (dashed green curves in Fig. 1), we see that the use of dominant mode templates with nonprecessing spins enhances the effectualness in detecting nonspinning signals containing subdominant modes, thus reducing the region in the parameter space where subdominant mode templates are required for detection. However, this is achieved at the cost of introducing larger systematic errors in the estimated parameters, thus increasing the volume of the parameter space where subdominant mode templates should be used in the parameter estimation.

This effect (better effectualness at the cost of larger systematic errors) is more pronounced in the case of binaries with spins *anti-aligned* with the orbital angular momentum. Thus, subdominant templates are required for detection of binaries with anti-aligned spins only over a small region in the parameter space; but they are required for parameter estimation over a large region. This effect is reversed in the case of *aligned* spins.

The rest of this paper is organized as follows: Sec. II provides details of the methodology and figures of merit for this study. Sec. III discusses our results including how we arrive at Fig. 1. Finally, Sec. IV has some concluding remarks, limitations of this work and targets for future work. Please note our notation for the rest of this article: M refers to the total mass of the binary, m_1 and m_2 refer to the component masses, χ_1 and χ_2 refer to the dimensionless spin parameters; $\chi_{1,2} = S_{1,2}/m_{1,2}^2$ where $S_{1,2}$ are the spin angular momenta of the components. We only consider spins aligned/anti-aligned with the orbital angular momentum. The mass ratio is denoted by $q = m_1/m_2$ while $\eta = m_1 m_2/M^2$ denotes the symmetric mass ratio. We also define the effective spin parameters $\chi_{\rm eff} = (m_1\chi_1 + m_2\chi_2)/M$ and $\tilde\chi_{\rm eff} = (m_1\chi_1 - m_2\chi_2)/M$. We refer to waveforms that include contributions from sub-dominant modes ($\ell \leq 4$, $m \neq 0$) as "full" waveforms, and waveforms that include only quadrupole modes ($\ell = 2, m = \pm 2$) as "quadrupole" waveforms. We refer to the SNR averaged over orientation and inclination angles as the orientation-averaged SNR, note that SNR along optimal orientation is ~ 2.5 times the orientation-averaged SNR [21].

previous study of nonspinning binaries to the case of spinning binaries with equal component spins. Our new study covers a larger region in the parameter space (higher mass ratios and spins) that they consider. They also use a template family with a single effective aligned spin parameter limited to $\chi_{\rm eff} < 0.6$. As we use a template family with two aligned spin parameters, we see better fitting factors at the cost of a larger parameter bias.

Simulation ID	q	χ_{1z}	χ_{2z}	$M\omega_{\mathrm{orb}}$	# orbits
SXS:BBH:0172	1	0.98	0.98	0.015	25.4
SXS:BBH:0090	1	0.00	0.00	0.011	32.4
SXS:BBH:0156	1	−0.95	−0.95	0.016	12.4
SXS:BBH:0253	2	0.50	0.50	0.014	28.8
SXS:BBH:0184	2	0.00	0.00	0.018	15.6
SXS:BBH:0238	2	−0.50	−0.50	0.011	32.0
SXS:BBH:0047	3	0.50	0.50	0.017	22.7
SXS:BBH:0174	3	0.50	0.00	0.013	35.5
SXS:BBH:0183	3	0.00	0.00	0.020	15.6
SXS:BBH:0036	3	−0.50	0.00	0.012	31.7
SXS:BBH:0046	3	−0.50	−0.50	0.018	14.4
SXS:BBH:0167	4	0.00	0.00	0.021	15.6
SXS:BBH:0110	5	0.50	0.00	0.019	24.2
SXS:BBH:0056	5	0.00	0.00	0.016	28.8
SXS:BBH:0109	5	−0.50	0.00	0.020	14.7
SXS:BBH:0181	6	0.00	0.00	0.018	26.5
SXS:BBH:0202	7	0.60	0.00	0.013	62.1
SXS:BBH:0203	7	0.40	0.00	0.013	58.5
SXS:BBH:0298	7	0.00	0.00	0.021	19.7
SXS:BBH:0205	7	−0.40	0.00	0.013	44.9
SXS:BBH:0207	7	−0.60	0.00	0.014	36.1
SXS:BBH:0065	8	0.50	0.00	0.019	34.0
SXS:BBH:0063	8	0.00	0.00	0.019	25.8
SXS:BBH:0064	8	−0.50	0.00	0.020	19.2
SXS:BBH:0189	9.2	0.00	0.00	0.021	25.2
SXS:BBH:0185	10	0.00	0.00	0.021	24.9

TABLE I: Summary of the parameters of the NR waveforms used in this paper: $q \equiv m_1/m_2$ is the mass ratio of the binary, χ_{1z} and χ_{2z} are the dimensionless spins of the larger and smaller black holes respectively, and $M\omega_{\mathrm{orb}}$ is the orbital frequency after the junk radiation. All of these waveforms have residual eccentricity, $e < 4 \times 10^{-3}$ (typically significantly smaller).

II. METHODOLOGY

In a past study [13], we investigated the effects of non-quadrupole modes in the detection and parameter estimation of nonspinning binaries. Here we extend the earlier work to the case of nonprecessing binaries, covering a wide range of total masses ($40M_\odot \leq M \leq 300M_\odot$), mass ratios ($q \leq 10$) and spins ($-0.5 \lesssim \chi_{\mathrm{eff}} \lesssim 0.5$). As our target signals, we use hybrid waveforms constructed by matching NR waveforms that describe the late inspiral, merger and ringdown of binary black holes with post-Newtonian (PN) / effective-one-body (EOB) waveforms modeling the early inspiral. These hybrids contain all the relevant modes ($h_{\ell m}(t)$ with $\ell \leq 4, |m| \leq \ell, m \neq 0$) of GW signals from binary black holes. The PN waveforms were generated using the 3PN amplitude given by [22–24], but using the phase evolution given by the SEOBNRv2 waveform family[2] [25]. We match them with NR waveforms produced by the SpEC [26–41] code by the SXS collaboration that are available at the public SXS catalog of NR waveforms [26]. The parameters of the NR waveforms used in this study are shown in Table I and Fig. 2. Note that the $(\ell, m) = (4,1)$ mode in several of the NR waveforms has significant numerical noise. However, as the amplitude of this mode is several orders of

magnitude smaller than that of the dominant mode, we do not expect this to impact our results.

As described in detail in our past study [13], to construct hybrids, we match the PN modes $h_{\ell m}^{\mathrm{PN}}(t)$ with NR modes $h_{\ell m}^{\mathrm{NR}}(t)$ by a least square fit over two rotations (φ_0, ψ) on the NR mode and the time-difference between NR and PN modes:

$$\Delta = \min_{t_0, \varphi_0, \psi} \int_{t_1}^{t_2} dt \sum_{\ell, m} \left| h_{\ell m}^{\mathrm{NR}}(t - t_0) e^{i(m\varphi_0 + \psi)} - h_{\ell m}^{\mathrm{PN}}(t) \right|. \tag{2.1}$$

The hybrid modes are constructed by combining the NR modes with the "best matched" PN modes:

$$h_{\ell m}^{\mathrm{hyb}}(t) \equiv \tau(t)\, h_{\ell m}^{\mathrm{NR}}(t - t_0')\, e^{i(m\varphi_0' + \psi')} + (1 - \tau(t))\, h_{\ell m}^{\mathrm{PN}}(t), \tag{2.2}$$

where t_0', φ_0' and ψ' are the values of t_0, φ_0 and ψ that minimizes the difference Δ between PN and NR modes, and, $\tau(t)$ is a suitable weighting function that smoothly goes from 0 to 1 during the interval $t_1 \leq t \leq t_2$. We refer the reader to [13] for details about construction of hybrid waveforms. An example of hybrid waveform modes is shown in Fig. 3. It can be seen that higher modes are excited only during the very late inspiral, merger and ringdown. The effect of higher modes will be appreciable only in the mass range where the SNR contributed by the merger-ringdown is a significant fraction of the total SNR. This is the reason we restrict our study to the mass range $40M_\odot \leq M \leq 300M_\odot$; we do not see any evidence of significant impact of higher modes for binaries with lower masses. Since the NR waveforms we use include 10s of cycles in the inspiral, we do not expect hybridization errors to impact our results, particularly for high masses. For a detailed study on hybridization errors we refer the reader to [42–46].

The template family used is IMRPhenomD, which is a quadrupole-only ($\ell = 2, m = \pm 2$) inspiral, merger and ringdown waveform family described by two mass parameters and two nonprecessing spin parameters [47, 48]. These waveforms are calibrated to NR waveforms with $q \leq 18, |\chi_{1z,2z}| \lesssim 0.85$ (0.98 for $q = 1$) and we find that they have a very good agreement
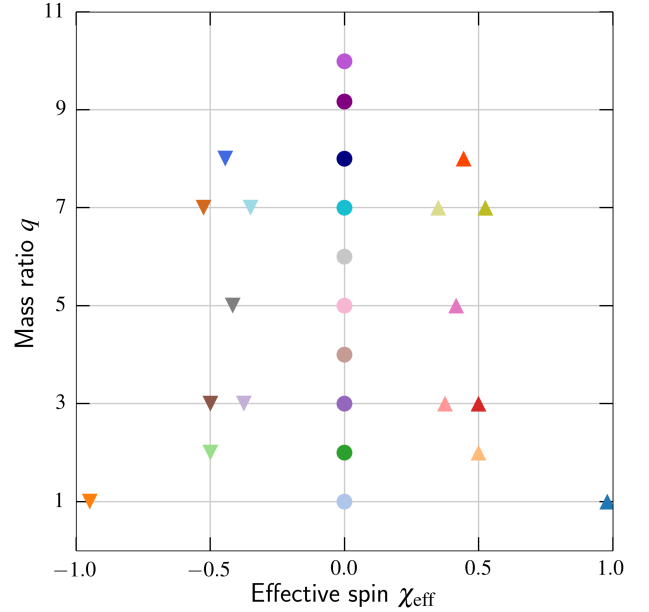

FIG. 2: This plot shows the mass ratio (vertical axis) and effective spin (horizontal axis) of the NR waveforms used in this study. The color scheme of the markers is same as that in Figs. 1, 6 and 8, enabling direct comparison.

---

[2] This was done in order to make the phase evolution of the hybrids very similar to that of the templates, so that a mismatch between the hybrid and the template due to the different phase evolution will not be mistaken as due to the effect of subdominant modes.
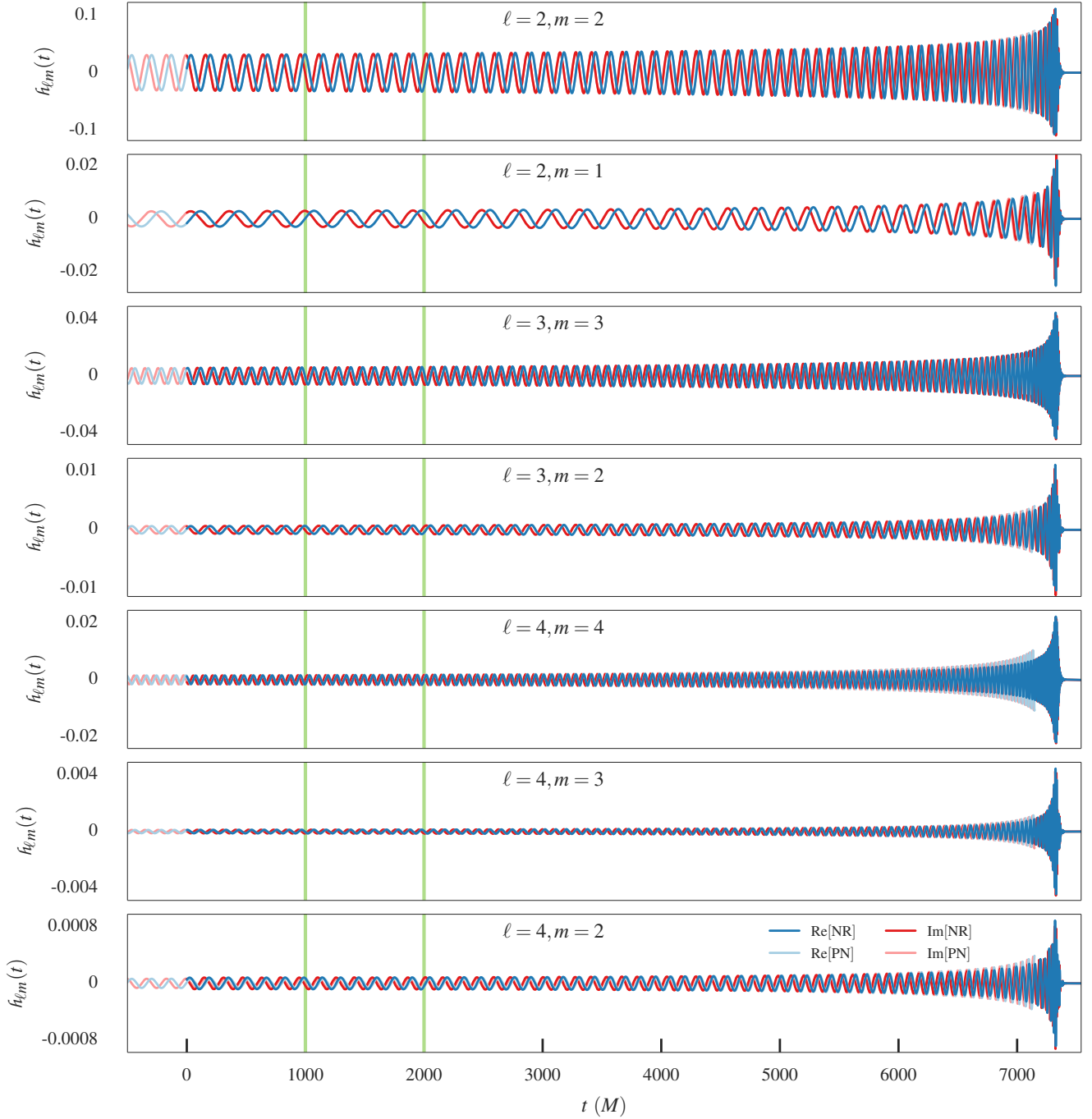
FIG. 3: Example of hybrid waveform modes constructed by matching NR and PN modes. These hybrid waveforms are constructed by matching $q = 8, \chi_{1z} = 0.5, \chi_{2z} = 0$ NR waveforms computed using the SpEC code with PN/EOB waveforms describing the early inspiral. The horizontal axes show the time (with origin at the start of the NR waveforms) and the vertical axes show the GW modes $\hat{h}_{\ell m}(t)$. The matching region $(1000M, 2000M)$ is marked by vertical green lines.

with the quadrupole modes of the hybrid waveforms discussed above (cf. the dashed lines in Fig. 6). The waveforms are generated in the Fourier-domain using the LALSimulation [49] software package.

We compute fitting factors [50] by maximizing the overlap (noise weighted inner product) of the template family against the target hybrid signals and infer the systematic errors by comparing the best match parameters with the true parameters. The overlaps are maximized over the extrinsic parameters (time of arrival t_0 and the reference phase φ_0) using the standard techniques in GW data analysis (see, e.g., [51]), while the overlaps are maximized over the intrinsic parameters $(M, \eta, \chi_{1z}$

and $\chi_{2z})$ of the templates using a Nelder-Mead downhill simplex algorithm [52], with additional enhancements described in [13]. As the model of the noise power spectrum, we use the "zero-detuned, high-power" design noise PSD [53] of Advanced LIGO with a low frequency cut-off of 20 Hz.

The contribution of subdominant modes in the observed signal depends on the relative orientation of the binary and the detector. The SNR (and hence the volume in the local universe where the binary can be confidently detected) is also a strong function of this relative orientation. For e.g., binaries that are face-on produce the largest SNR in the detector; however, the contribution from subdominant modes is minimal for this
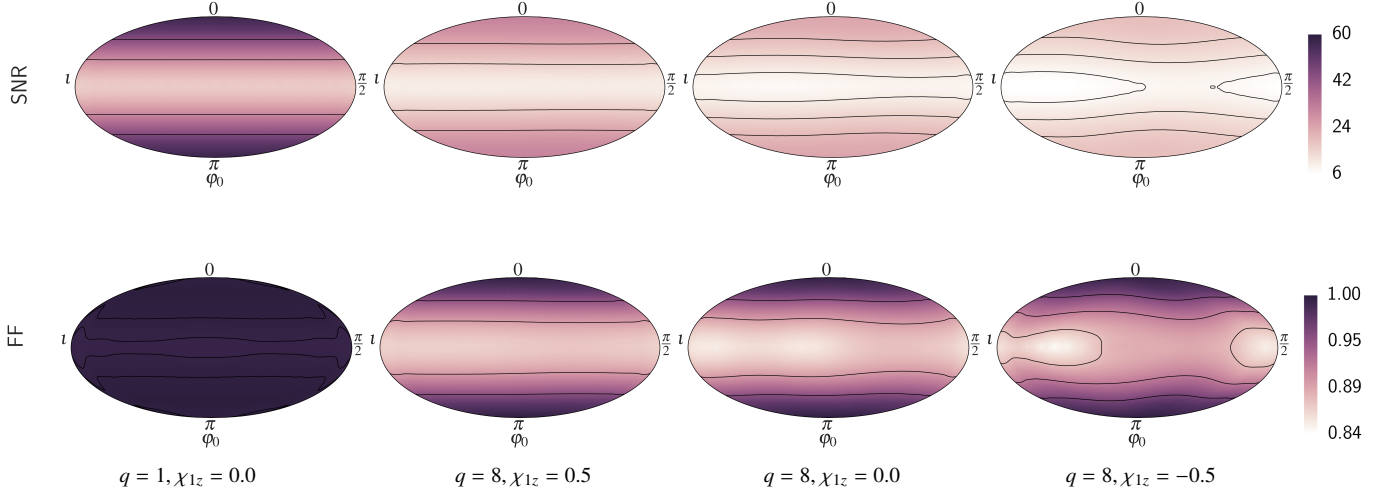
FIG. 4: Optimal SNR (top panel) and fitting factor of quadrupole templates (bottom panel), averaged over polarization angle ψ for binaries with total mass $M = 100\, M_\odot$, located at 1 Gpc. The y-axis shows the inclination angle ι in radians and the x-axis shows the initial phase of the binary φ_0 in radians. The equator ($\iota = \pi/2$) corresponds to "edge-on" orientation while the poles ($\iota = 0, \pi$) correspond to "face-on" orientation. Different columns correspond to different mass ratios and spin. It may be noted that the fitting factor as well as the intrinsic luminosity are smallest (largest) at $\iota = \pi/2$ ($\iota = 0, \pi$) where contribution from the non-quadrupolar modes is the largest (smallest), illustrating the selection bias towards configurations where non-quadrupole modes are less important.

orientation. This effect is reversed for the case of edge-on orientations. Thus, if we want to calculate the effect of subdominant modes on detection and parameter estimation of a population of binary black holes, the effect has to be averaged over all orientations after appropriately weighting each orientation.

We evaluate the *effective volume* [13] of a search, defined as the fraction of the volume that is accessible by an optimal search (corresponding to a fixed SNR threshold), by averaging over all the relative orientations in the following way:

$$V_{\text{eff}}(m_1, m_2, \chi_{1z}, \chi_{2z}) = \frac{\overline{\rho_{\text{opt}}^3 \, \text{FF}^3}}{\overline{\rho_{\text{opt}}^3}}, \qquad (2.3)$$

where ρ_{opt} is the optimal SNR of the full signal, FF is the fitting factor of the dominant mode template, and the bars indicate averages over all (isotropically distributed) orientations [3]. The dominant-mode template family is deemed effectual for detection when the effective volume is greater than 90%; or when the *effective fitting factor* $\text{FF}_{\text{eff}} := V_{\text{eff}}^{1/3}$ is greater than 0.965.

Similarly, we define the *effective bias* [13] in estimating an intrinsic parameter λ as

$$\Delta\lambda_{\text{eff}}(m_1, m_2, \chi_{1z}, \chi_{2z}) = \frac{\overline{|\Delta\lambda| \, \rho_{\text{opt}}^3 \, \text{FF}^3}}{\overline{\rho_{\text{opt}}^3 \, \text{FF}^3}}, \qquad (2.4)$$

where $\Delta\lambda$ is the systematic bias in estimating the parameter λ for one orientation, FF is the corresponding fitting factor, and

ρ_{opt} the corresponding optimal SNR. Here also the bars indicate averages over all orientations. The effective bias provides an estimate of the bias averaged over a population of detectable binaries with isotropic orientations. We compare them against the sky and orientation averaged statistical errors. Statistical errors are computed using the Fisher matrix formalism employing quadrupole-only templates. The quadrupole-mode template family is deemed faithful for parameter estimation when the effective biases in all of the three intrinsic parameters $M, \eta, \chi_{\text{eff}}$ are smaller than the 1σ statistical errors in measuring the same parameter for an orientation-averaged SNR of 8.

III. RESULTS AND DISCUSSION

In this section, we evaluate the performance of the quadrupole-mode inspiral-merger-ringdown template family IMRPhenomD, against the "full" hybrid waveforms by computing the fitting factor of the template and inferring the parameter biases from the best matched parameters. Figure 4 shows the optimal SNR of the hybrid waveforms and fitting factor of the quadrupole-mode templates at different values of ι and φ_0 (averaged over the polarization angle ψ). Figure 5 shows the systematic bias in estimating parameters total mass M, symmetric mass ratio η and effective spin χ_{eff}, using the quadrupole-mode template family. It is clear that for the $q = 1$ case (left column) the fitting factor is close to 1 and the systematic errors are negligible for all orientations, indicating the weak contribution of subdominant modes. For mass ratio 8, the fitting factor can be as low as ~ 0.84 for binaries that are highly inclined ($\iota \simeq \pi/2$) with the detector, where the contribution from non-quadrupole modes is the highest. However, these are the orientations where the SNR is the minimum (see Fig. 4). Similarly, the systematic biases are typically the largest (smallest) for the edge-on (face-on) configurations where the SNR is the smallest (largest). Hence GW observations are intrinsically biased towards orientations where the effect of non-quadrupole
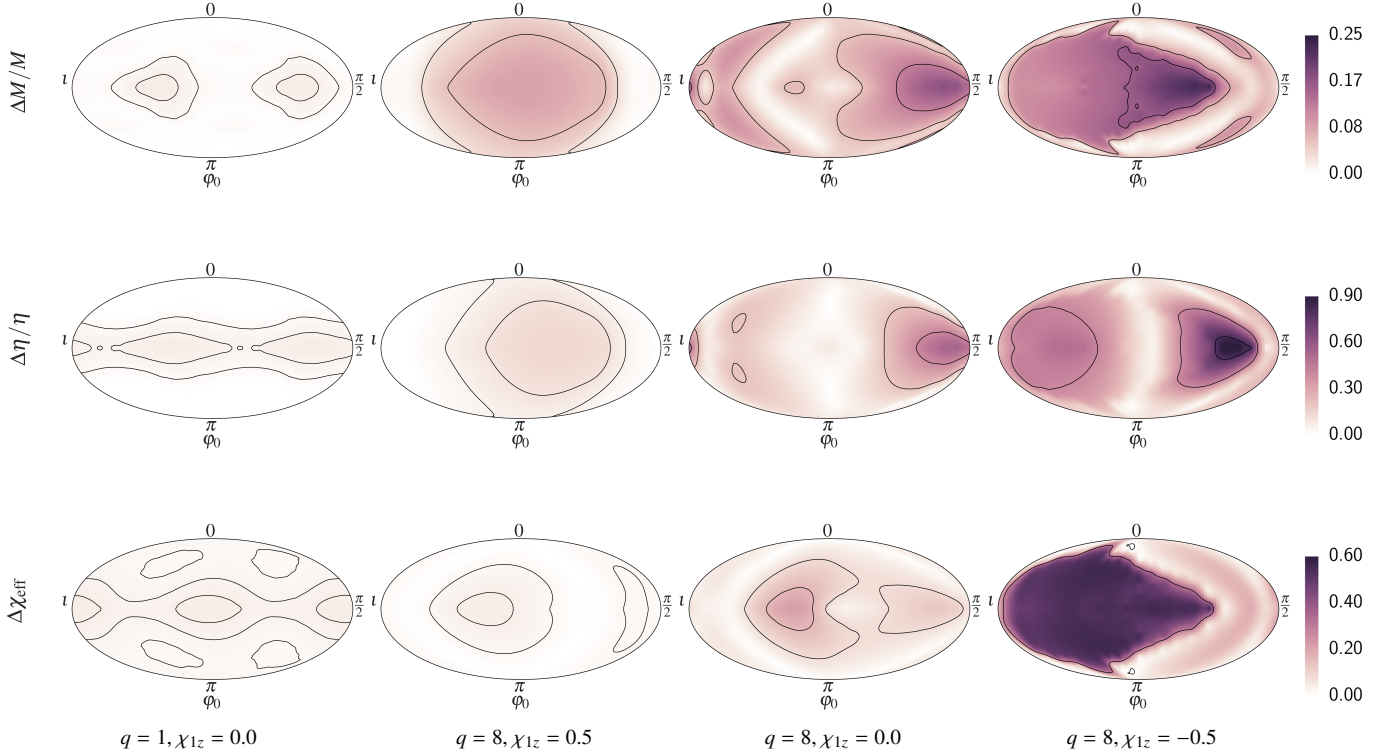
---

[3] This corresponds to uniform distributions in the phase angle $\varphi_0 \in [0, 2\pi)$, polarization angle $\psi \in [0, 2\pi)$, and the cosine of the inclination angle $\cos\iota \in [-1, 1]$. Note that we assume that the binaries are optimally located (i.e., the angles θ, ϕ describing the location of the binary in the detector frame on the sky are set to zero). The error introduced by this restriction is very small ($\sim 0.1\%$) due to the weak dependence of the matches on (θ, ϕ) and the strong selection bias towards binaries with $\theta \simeq 0, \pi$, where the antenna pattern function peaks [13].

FIG. 5: Systematic bias in the estimation of total mass M (top panel), symmetric mass ratio η (middle panel), and effective spin $\chi_{\rm eff}$ (bottom panel), averaged over polarization angle ψ for binaries with total mass $M = 100~M_\odot$. For M and η, relative biases are shown, while for $\chi_{\rm eff}$ absolute biases are shown. The y-axis shows the inclination angle ι in radians and the x-axis shows the initial phase of the binary φ_0 in radians. Different columns correspond to different mass ratios and spins.

modes is minimum. This effect, in general, reduces the importance of non-quadrupole modes for a population of binaries that are oriented isotropically [13, 15–17].

Figure 6a shows the *ineffectualness* $(1-{\rm FF}_{\rm eff})$ while Figs. 6b–6d show effective biases in estimated parameters as a function of the total mass of the binary for different mass ratios and spins. For total mass M and symmetric mass ratio η, fractional biases are shown while for $\chi_{\rm eff}$ absolute biases are shown[4]. Solid (dashed) lines correspond to the case where "full" (quadrupole-only) hybrid waveforms are used as target waveforms. The template family in both cases contains only the quadrupole mode. The difference between the solid and dashed lines indicates the effect of ignoring sub-dominant modes for detection and parameter estimation. Note that many of the dashed lines lie below the scale of these plots and are not displayed.

Previous studies [13, 15–17, 20] have shown that the effects of subdominant modes become important for binaries with high masses and large mass ratios. At large mass ratios, subdominant modes are excited by a larger extent due to higher asymmetry. For high masses, the observed signal is dominated by the merger, during which sub-dominant modes are excited prominently. Consistent with our expectation, in Fig. 6, the solid lines show that, in general, the ineffectualness and effective biases increase with increasing mass ratio and with increasing mass. We also see a clear separation of the solid and dashed lines in

Figs. 6a–6d for large mass ratios and high masses, illustrating the effect of neglecting non-quadrupole modes.

Figure 6a also reveals an interesting dependence of the effect of non-quadrupole modes on the spins. For binaries with aligned, zero, and anti-aligned spins, the ineffectualness peaks at total mass of $M \sim 300M_\odot$, $M \sim 150M_\odot$, $M \sim 100M_\odot$, respectively. This is roughly the mass range where the observed signal is dominated by the late inspiral and merger – the phase where the higher modes are excited most prominently. We remind the reader that, for binaries with anti-aligned spins, merger happens at relatively lower frequencies, while, for the case of aligned spins, merger happens at relatively higher frequencies, owing to the "orbital hangup" [54, 55] effect. Since frequencies are scaled inversely to the total mass of the system, this creates the mass dependence of the ineffectualness that we describe above. For very high masses, the observed signal will contain only the ringdown phase. Due to the smaller bandwidth and the relatively simpler structure of the ringdown signal, the quadrupole-only templates are likely to be able to mimic the full ringdown signal relatively well, at the cost of considerable systematic errors (see Fig. 7 for an example). Hence, we anticipate the effectualness of the quadrupole-mode templates to go up at very high masses. This effect should start dominating the effectualness patterns at relatively lower masses for binaries with anti-aligned spins. Consistent with our expectation, we see in Fig. 6a that that for a given mass ratio, at low masses, binaries with negative spins have higher ineffectualness but as the mass increases there is a crossover point beyond which binaries with positive spins have higher ineffectualness. While for positive spins, the ineffectualness continues to increase with total mass, for zero spins the ineffectualness plateaus and for negative spins it reaches a maximum value and starts deceasing

---

[4] In the case of anti-symmetric spin parameter $\tilde\chi_{\rm eff}$, the biases are dominated by the bias in the quadrupole mode itself. This is expected as previous studies have shown that LIGO can only estimate $\chi_{\rm eff}$ to a good accuracy. Therefore we do not consider biases in $\tilde\chi_{\rm eff}$ in this study.

(a) Ineffectualness

(b) Effective bias in M

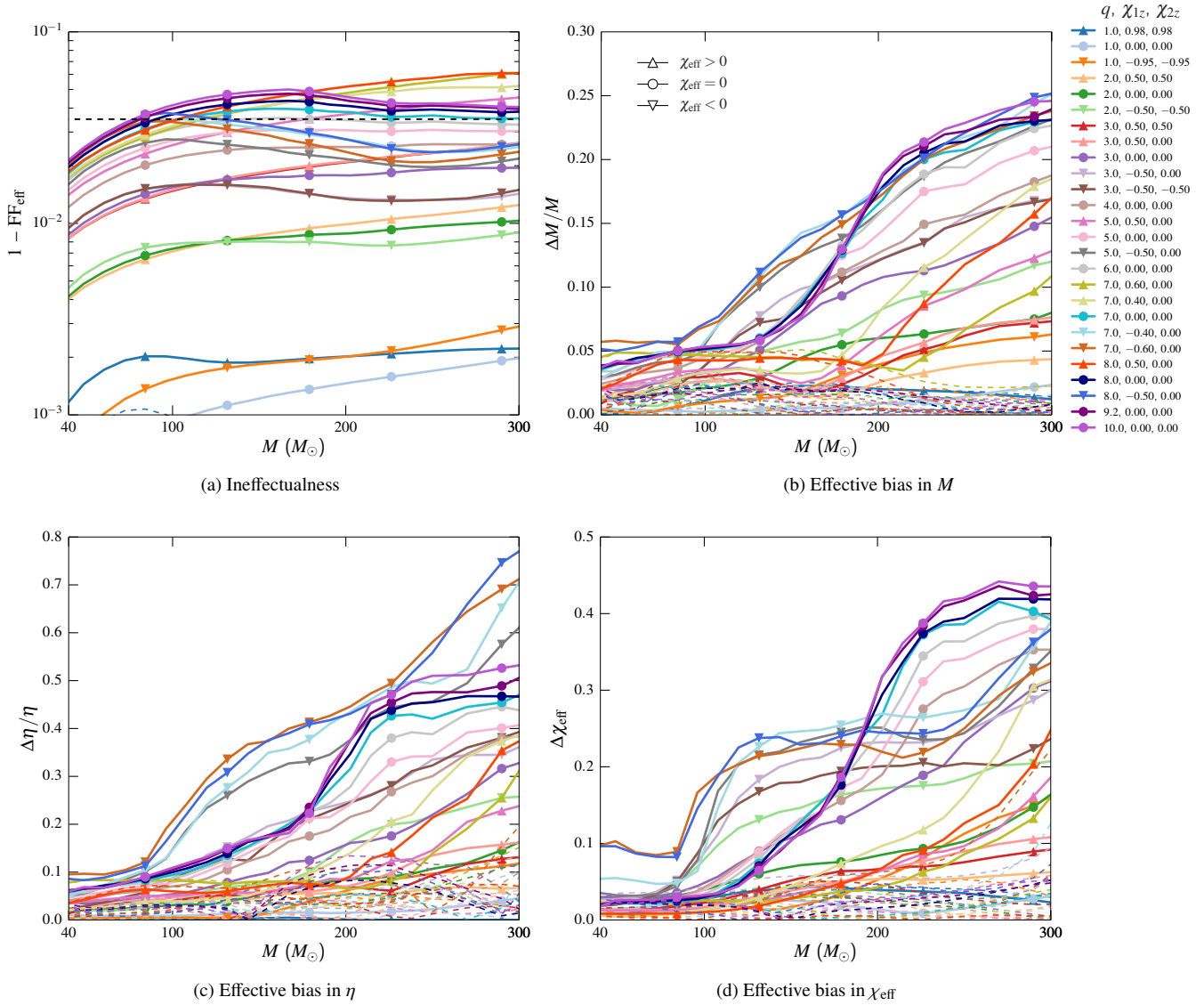(c) Effective bias in η

(d) Effective bias in χ_{eff}

FIG. 6: "Ineffectualness" (1 - FF_{eff}) and effective parameter biases when using quadrupole mode templates against "full" hybrid waveforms. Dashed lines correspond to the same but against quadrupole-only hybrid waveforms. Fractional biases are shown for total mass M and symmetric mass ratio η, while absolute biases are shown for effective spins χ_{eff}. FF_{eff} and effective parameter biases are obtained by averaging over all relevant orientations of the binary using Eqs. (2.3) and (2.4). The horizontal axis reports the total mass of the binary while the mass ratio and spins are shown in the legend. The markers indicate the spin types: triangles pointing up/down denoting binaries with aligned/anti-aligned spins and circles denoting nonspinning binaries. The horizontal dashed black line corresponds to $1 - FF_{\text{eff}}^3 = 0.1$. Note that most of the dashed lines in the top-left subplot lie below 10^{-3}. We see that as the total mass increases, the ineffectualness and effective biases in M, η and χ_{eff} increase and are dominated by the effects of subdominant modes; see Sec. III for further discussion.

beyond that point. We see from Figs. 6b–6d that this trend of larger (smaller) effectualness for negative (positive) spins at high masses ($M \gtrsim 100 M_{\odot}$) is achieved at the cost of larger (smaller) systematic biases in the estimated parameters.

We set $FF_{\text{eff}} \geq 0.965$ (which corresponds to a $\sim 10\%$ loss in detection volume for a fixed SNR threshold) as the benchmark for the relative importance of non-quadrupole modes in detection. This is shown by the dashed black line in Fig. 6a. Fig. 1a summarizes the region in the parameter space where the loss of detectable volume (at a fixed SNR threshold) due to neglecting non-quadrupole modes is greater than 10%. For the case of negative spins, even at large mass ratios, we see that subdominant modes are important for detection only over a range of masses ($M \sim 75 - 150 M_{\odot}$). For binaries with positive and zero

spins, we anticipate that the upper limit of total mass where the higher modes are important are above $300 M_{\odot}$, the highest mass that we consider in this study. Based on Fig. 1a, we expect the quadrupole mode templates to be fully effectual for detection either when $q \lesssim 4$ or when $M \lesssim 70 M_{\odot}$ (irrespective of spins), considering a population of binaries distributed with isotropic orientations. We note that the region in which subdominant modes become important for detection is the smallest (largest) for negative (positive) spins.

Figure 1a also shows the region in the parameter space (marked by the green dashed line) where subdominant modes are important for the detection of nonspinning binaries when nonspinning quadrupole mode templates are used, obtained in our previous study [13]. We see that the use of quadrupole
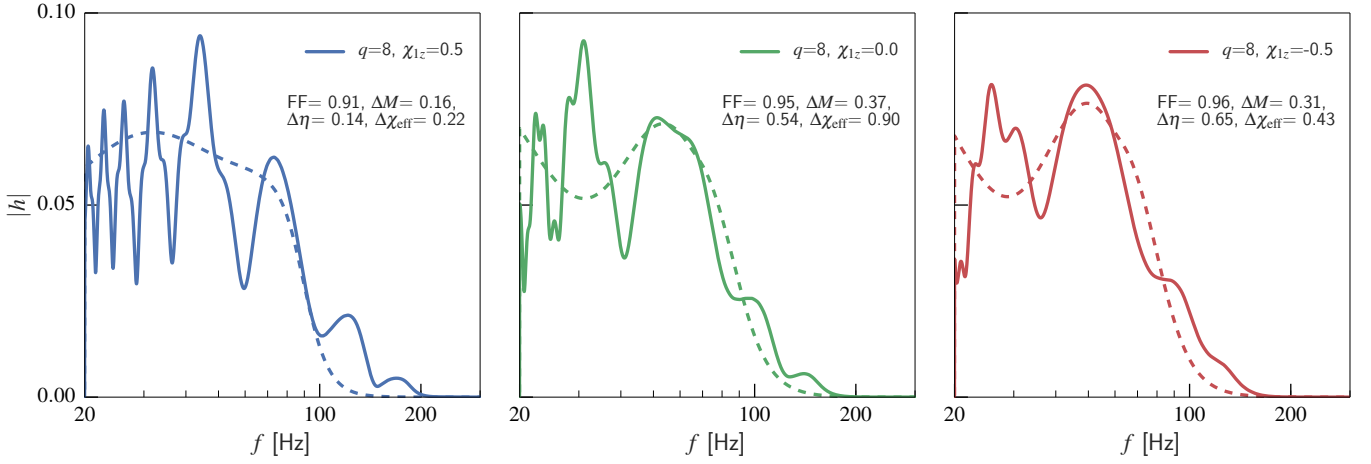
FIG. 7: Comparison of the frequency domain amplitudes of the "full" hybrid waveform containing subdominant modes (solid lines) and the best match template waveforms containing only the quadrupole modes (dashed lines). The waveforms have been "whitened" according to the PSD used for match calculation. The orientation angles are chosen to be $\iota = \pi/4$, $\varphi_0 = \pi$, $\psi = \pi/3$. The total mass is $M = 200\,M_\odot$ and mass ratio is $q = 8$. The legends show the spin of the larger black hole. The spin on the smaller black hole is zero in all three cases. The inset text shows the fitting factor, fractional biases in parameters M and η and absolute bias in parameter χ_{eff}, at the best match point. Particularly in the case of negative spin, where the observed signal is dominated by the ringdown, we see that the template is able to mimic the target, producing reasonably good fitting factor. But this comes at the expense of larger parameter biases.
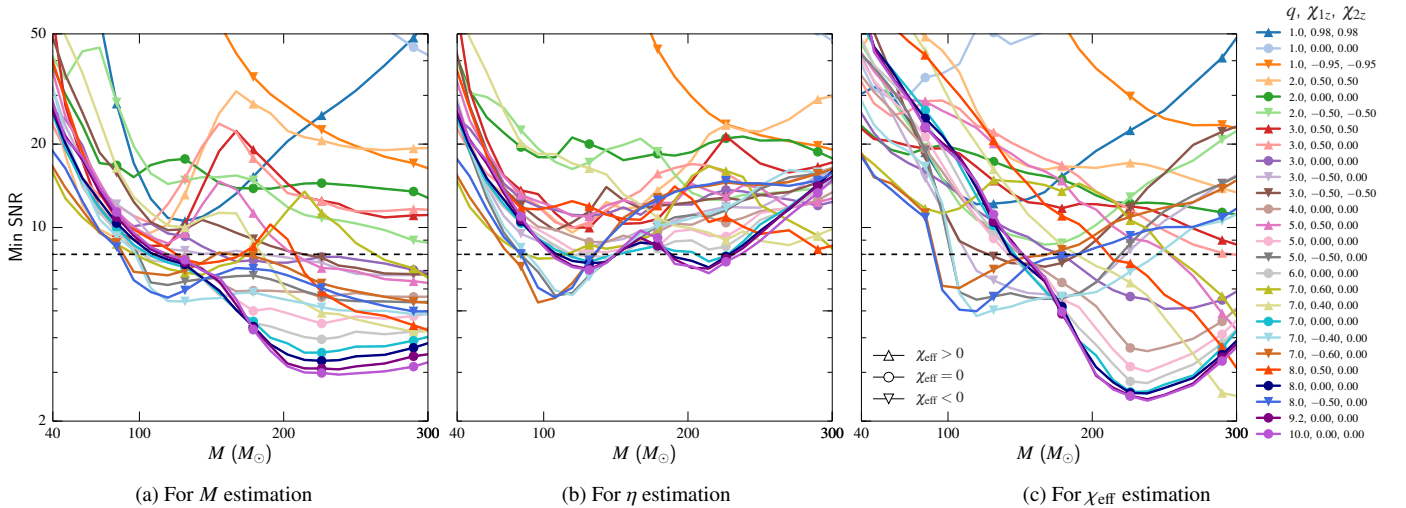

(a) For M estimation　　(b) For η estimation　　(c) For χ_{eff} estimation

FIG. 8: Minimum orientation-averaged SNR at which the statistical errors are low enough to equal the effective systematic bias in parameters M, η and χ_{eff}, when using quadrupole mode templates and "full" hybrid waveforms as the target signals. A dashed black line is used to denote minimum orientation-averaged SNR of 8 (optimal orientation SNR of 20).

mode templates with nonprecessing spins have helped us to reduce the region in the parameter space where subdominant modes cause unacceptable loss in the detection volume. This is consistent with our expectation, as two additional parameters (spins) in the templates allow them to achieve higher fitting factors with the target signals, at the cost of a larger bias in the best matched template parameters.

In order to gauge the relative importance of the systematic errors shown in Figs. 6b–6d, we compare them against the expected statistical errors from the quadrupole-mode template family IMRPhenomD (computed using Fisher matrix formalism). Figure 8 shows the minimum SNR (orientation-averaged) at which the $1\,\sigma$ statistical errors become low enough to equal the systematic errors. (Note that statistical errors are inversely proportional to the SNR.) We see that, at high masses,

the systematic errors start to dominate the error budget for orientation-averaged SNRs as low as 3. In this study, whenever the systematic errors are less than the statistical error for an orientation-averaged SNR of 8 (horizontal black dashed line in Fig. 8), we regard the quadrupole-mode templates to be faithful for parameter estimation [5].

Figure 1b summarizes the region in the parameter space where this minimum orientation-averaged SNR is less than or equal to 8 for estimation of any of M, η or χ_{eff}. We exclude

_____

[5] Note that, when full mode templates are employed in the parameter estimation, the statistical errors are expected to go down in general, due to the increased amount of information in the waveform (see, e.g., [56]). We do not consider this effect here.

any cases where the systematic biases are dominated by the biases in the quadrupole mode itself. We note that the region in which subdominant modes become important for parameter estimation is smallest (largest) for positive (negative) spins. This trend is opposite to what we see in Fig. 1a for detection. This is because, at high masses negative spin binaries have higher effectualness than positive spin binaries, which is achieved at the cost of higher systematic biases. We remind the reader that, for spins of higher magnitude than considered in this study (i.e. $|\chi_{\text{eff}}| > 0.5$), we expect the shaded regions in Fig. 1 to expand or reduce depending on the spin; the contours that we draw are indicative demarcations only. For greater aligned spins, the shaded region for detection should expand and the shaded region for parameter estimation should reduce. The opposite trend is expected for greater anti-aligned spins. Figure 1b also compares these results with the results obtained in our previous study [13] (dashed green line) using nonspinning quadrupole-only templates against nonspinning "full" target waveforms. We see that the use of spinning templates essentially increases the region where the parameter estimation bias is dominated by systematic errors.

IV. CONCLUSION

We studied the effects of sub-dominant modes in the detection and parameter estimation of GWs from black hole binaries with nonprecessing spins using Advanced LIGO detectors. The effect of sub-dominant modes on detection is quantified in terms of the effective detection volume (fraction of the optimal detection volume that the suboptimal search is sensitive to, for a given SNR threshold) and the effect on parameter estimation in terms of the effective bias (weighted average of the systematic errors for different orientations) in the estimated parameters. We compared quadrupole-mode templates with target signals (hybrid waveforms constructed by matching NR simulations describing the late inspiral, merger and ringdown with PN/EOB waveforms describing the early inspiral). These signals contained contributions from all the spherical harmonic modes up to $\ell = 4$ and $-\ell \leq m \leq \ell$ except the $m = 0$ modes.

Our study considered black hole binaries with total masses $40 M_\odot \leq M \leq 300 M_\odot$, mass ratios $1 \leq q \leq 10$, various spins including $\chi_{\text{eff}} \sim -0.5, 0, 0.5$. The results are appropriately averaged over all angles describing the orientation of the binary. Fig. 1 shows the regions in the parameter space where the contribution from non-quadrupole modes is important for GW detection and parameter estimation. In general, neglecting subdominant modes can cause unacceptable loss of SNR and unacceptably large systematic errors for binaries with high masses and large mass ratios. For a given mass ratio, subdominant modes are more important for positive (negative) spins for detection (parameter estimation). As compared to our previous study restricted to the case of nonspinning binaries, we see that the use of quadrupole mode templates with nonprecessing spins, enhances the effectualness for detection, but extends the region where systematic errors dominate.

Note that the scope of our study was rather restricted – while we conclude that subdominant mode templates are likely to improve the detection rates of binary black holes in certain regions in the parameter space (high mass and large mass ratios), a proper characterization of this will require characterizing the associated increase in the false alarm rate also (see, e.g., [17]). Also, we did not study the effect of neglecting nonquadrupole modes on signal-based vetoes such as the "chi-square" veto [57]. Similarly, we have only investigated the region in the parameter space where the use of quadrupole-only template would introduce systematic errors that are larger than the expected statistical errors. However, the use of full-mode templates in parameter estimation is likely to reduce the statistical errors, owing to the increased information content in the waveform. We have not explored this aspect of the problem here. The expected statistical errors were estimated using the Fisher matrix formalism. Since these error bounds are lower limits, our estimates on the region of the parameter space where the systematic errors are negligible should be treated as conservative estimates. We conclude that subdominant modes are important for parameter estimation when the systematic errors are greater than 1σ statistical errors at a sky and orientation averaged SNR of 8. If a more stringent criteria is applied, our shaded regions in Fig. 1b would widen. Also, note that we restricted our study to the case of binaries with nonprecessing spins. Astrophysical black hole binaries may have generic spin orientations. It is not clear how our conclusions hold in the case of precessing spins (see [58] for some recent work in this direction). We leave some of these investigations as future work.

[1] B. P. Abbott et al. (LIGO Scientific Collaboration and Virgo Collaboration), Phys. Rev. Lett. **116**, 061102 (2016), URL http://link.aps.org/doi/10.1103/PhysRevLett.116.061102.

[2] B. P. Abbott et al. (LIGO Scientific Collaboration and Virgo Collaboration), Phys. Rev. Lett. **116**, 241103 (2016), URL http://link.aps.org/doi/10.1103/PhysRevLett.116.241103.

[3] B. P. Abbott et al. (LIGO Scientific Collaboration), ArXiv e-prints (2016), 1602.03842.

[4] B. P. Abbott et al. (LIGO Scientific Collaboration and Virgo Collaboration), Phys. Rev. X **6**, 041015 (2016), URL http://link.aps.org/doi/10.1103/PhysRevX.6.041015.

[5] B. P. Abbott et al. (LIGO Scientific Collaboration and Virgo Collaboration), Phys. Rev. Lett. **116**, 241102 (2016), URL http://link.aps.org/doi/10.1103/PhysRevLett.116.241102.

[6] B. P. Abbott et al. (LIGO Scientific Collaboration), The Astrophysical Journal Letters **818**, L22 (2016), 1602.03846.

[7] B. P. Abbott et al. (LIGO Scientific and Virgo Collaborations), Phys. Rev. Lett. **116**, 221101 (2016), URL http://link.aps.org/doi/10.1103/PhysRevLett.116.221101.

[8] S. Klimenko et al., Phys. Rev. **D93**, 042004 (2016), 1511.05999.

[9] S. Klimenko, I. Yakushin, A. Mercer, and G. Mitselmakher, Classical and Quantum Gravity **25**, 114029 (2008), URL http://stacks.iop.org/0264-9381/25/i=11/a=114029.

[10] B. P. Abbott et al. (LIGO Scientific Collaboration and Virgo Collaboration), Phys. Rev. D **93**, 122004 (2016), URL http://link.aps.org/doi/10.1103/PhysRevD.93.122004.

[11] B. P. Abbott et al. (LIGO Scientific Collaboration and Virgo Collaboration), Phys. Rev. D **93**, 122003 (2016), URL http://link.aps.org/doi/10.1103/PhysRevD.93.122003.

[12] T. Damour, B. R. Iyer, and B. S. Sathyaprakash, Phys. Rev. D **57**, 885 (1998).

[13] V. Varma, P. Ajith, S. Husa, J. C. Bustillo, M. Hannam, and M. Pürrer, Phys. Rev. D **90**, 124004 (2014), URL http://link.aps.org/doi/10.1103/PhysRevD.90.124004.

[14] B. P. Abbott et al. (Virgo, LIGO Scientific), Phys. Rev. D **94**, 064035 (2016), 1606.01262.

[15] L. Pekowsky, J. Healy, D. Shoemaker, and P. Laguna, Phys. Rev. D **87**, 084008 (2013).

[16] D. A. Brown, P. Kumar, and A. H. Nitz, Phys. Rev. D **87**, 082004 (2013).

[17] C. Capano, Y. Pan, and A. Buonanno (2013), 1311.1286.

[18] B. P. Abbott et al. (the Virgo, The LIGO Scientific) (2016), 1611.07531.

[19] B. P. Abbott et al. (LIGO Scientific Collaboration and Virgo Collaboration), Phys. Rev. D **94**, 064035 (2016), URL http://link.aps.org/doi/10.1103/PhysRevD.94.064035.

[20] J. Calderón Bustillo, S. Husa, A. M. Sintes, and M. Pürrer, Phys. Rev. D **93**, 084019 (2016), URL http://link.aps.org/doi/10.1103/PhysRevD.93.084019.

[21] B. Sathyaprakash and B. F. Schutz, Living Reviews in Relativity **12** (2009), URL http://www.livingreviews.org/lrr-2009-2.

[22] L. Blanchet, G. Faye, B. R. Iyer, and S. Sinha, Class.Quant.Grav. **25**, 165003 (2008), 0802.1249.

[23] K. G. Arun, A. Buonanno, G. Faye, and E. Ochsner, Phys. Rev. D **79**, 104023 (2009), URL http://link.aps.org/doi/10.1103/PhysRevD.79.104023.

[24] A. Buonanno, G. Faye, and T. Hinderer, Phys. Rev. **D87**, 044009 (2013), 1209.6349.

[25] A. Taracchini, A. Buonanno, Y. Pan, T. Hinderer, M. Boyle, D. A. Hemberger, L. E. Kidder, G. Lovelace, A. H. Mroué, H. P. Pfeiffer, et al., Phys. Rev. D **89**, 061502 (2014), URL http://link.aps.org/doi/10.1103/PhysRevD.89.061502.

[26] SXS Gravitational Waveform Database, URL http://www.black-holes.org/waveforms/.

[27] The Spectral Einstein Code, URL http://www.black-holes.org/SpEC.html.

[28] A. H. Mroue, M. A. Scheel, B. Szilagyi, H. P. Pfeiffer, M. Boyle, et al. (2013), 1304.6077.

[29] A. H. Mroue and H. P. Pfeiffer (2012), 1210.2958.

[30] G. Lovelace, M. Scheel, and B. Szilagyi, Phys.Rev. **D83**, 024010 (2011), 1010.2777.

[31] J. Blackman, S. E. Field, C. R. Galley, B. Szilagyi, M. A. Scheel, M. Tiglio, and D. A. Hemberger, Phys. Rev. Lett. **115**, 121102 (2015), 1502.07758.

[32] L. T. Buchman, H. P. Pfeiffer, M. A. Scheel, and B. Szilagyi, Phys.Rev. **D86**, 084033 (2012), 1206.3015.

[33] S. Ossokine, L. E. Kidder, and H. P. Pfeiffer, Phys.Rev. **D88**, 084031 (2013), 1304.3067.

[34] D. A. Hemberger, M. A. Scheel, L. E. Kidder, B. Szilagyi, G. Lovelace, et al., Class.Quant.Grav. **30**, 115001 (2013), 1211.6079.

[35] B. Szilagyi, L. Lindblom, and M. A. Scheel, Phys.Rev. **D80**, 124010 (2009), 0909.3557.

[36] M. Boyle and A. H. Mroue, Phys.Rev. **D80**, 124045 (2009), 0905.3177.

[37] M. A. Scheel, M. Boyle, T. Chu, L. E. Kidder, K. D. Matthews, et al., Phys.Rev. **D79**, 024003 (2009), 0810.1767.

[38] M. Boyle et al., Phys. Rev. **D76**, 124038 (2007), 0710.0158.

[39] M. A. Scheel, H. P. Pfeiffer, L. Lindblom, L. E. Kidder, O. Rinne, et al., Phys.Rev. **D74**, 104006 (2006), gr-qc/0607056.

[40] L. Lindblom, M. A. Scheel, L. E. Kidder, R. Owen, and O. Rinne, Class.Quant.Grav. **23**, S447 (2006), gr-qc/0512093.

[41] H. P. Pfeiffer, L. E. Kidder, M. A. Scheel, and S. A. Teukolsky, Comput.Phys.Commun. **152**, 253 (2003), gr-qc/0202096.

[42] I. MacDonald, A. H. Mroue, H. P. Pfeiffer, M. Boyle, L. E. Kidder, M. A. Scheel, B. Szilagyi, and N. W. Taylor, Phys. Rev. **D87**, 024009 (2013), 1210.3007.

[43] I. MacDonald, S. Nissanke, H. P. Pfeiffer, and H. P. Pfeiffer, Class. Quant. Grav. **28**, 134002 (2011), 1102.5128.

[44] M. Hannam, S. Husa, U. Sperhake, B. Bruegmann, and J. A. Gonzalez, Phys. Rev. **D77**, 044020 (2008), 0706.1305.

[45] P. Ajith, Class. Quant. Grav. **25**, 114033 (2008).

[46] M. Hannam, S. Husa, F. Ohme, and P. Ajith, Phys. Rev. **D82**, 124052 (2010), 1008.2961.

[47] S. Khan, S. Husa, M. Hannam, F. Ohme, M. Pürrer, X. J. Forteza, and A. Bohé, Phys. Rev. D **93**, 044007 (2016), URL http://link.aps.org/doi/10.1103/PhysRevD.93.044007.

[48] S. Husa, S. Khan, M. Hannam, M. Pürrer, F. Ohme, X. J. Forteza, and A. Bohé, Phys. Rev. D **93**, 044006 (2016), URL http://link.aps.org/doi/10.1103/PhysRevD.93.044006.

[49] LALSimulation is part of the LALSuite software package, URL https://www.lsc-group.phys.uwm.edu/daswg/projects/lalsuite.html.

[50] T. A. Apostolatos, Phys. Rev. D **52**, 605 (1995).

[51] B. Allen, W. G. Anderson, P. R. Brady, D. A. Brown, and J. D. E. Creighton, Phys. Rev. **D85**, 122006 (2012), gr-qc/0509116.

[52] The SciPy software library, URL http://scipy.org/.

[53] *Advanced LIGO anticipated sensitivity curves*, LIGO Document T0900288-v3, URL https://dcc.ligo.org/LIGO-T0900288/public.

[54] M. Campanelli, C. O. Lousto, and Y. Zlochower, Phys. Rev. D **74**, 041501 (2006), URL http://link.aps.org/doi/10.1103/PhysRevD.74.041501.

[55] M. Hannam, S. Husa, B. Brügmann, and A. Gopakumar, Phys. Rev. D **78**, 104007 (2008), URL http://link.aps.org/doi/10.1103/PhysRevD.78.104007.

[56] C. Van Den Broeck and A. S. Sengupta, Class.Quant.Grav. **24**, 155 (2007), gr-qc/0607092.

[57] B. Allen, Phys. Rev. **D71**, 062001 (2005), gr-qc/0405045.

[58] J. C. Bustillo, P. Laguna, and D. Shoemaker, p. 6 (2016), 1612.02340, URL http://arxiv.org/abs/1612.02340.